ACS NANO
Cite This: ACS Nano 2018, 12, 9309–9317
www.acsnano.org

ARTICLE

Controlling Interlayer Spacing of Graphene Oxide Membranes by External Pressure Regulation

Wanbin Li,* Wufeng Wu, and Zhanjun Li

School of Environment and Guangdong Key Laboratory of Environmental Pollution and Health, Jinan University, Guangzhou 511443, P. R. China

Supporting Information

ABSTRACT: Graphene oxide (GO) membranes have been attracting numerous attention due to their impressive performance in various applications, especially in water purification. However, because the swelling in water and polar organic solvents causes the increase of interlayer channels, GO membranes usually possess inferior rejection for subnanometer-sized molecules. How to control the transport channels of GO membranes at angstrom level is a significantly scientific and practical issue. Herein, a concept of external pressure regulation (EPR) is reported for restraining GO swelling and controlling its interlayer spacing precisely. Since anisotropic GO films only swell at vertical direction, the interlayer channels can be manipulated by externally unidirectional reverse force. Based on this concept, an EPR system with GO membranes is designed for water desalination by adjusting the external pressure that has high resolution. In cross-flow filtration, the compressed GO membranes show high KCl, NaCl, and $CaCl_2$ rejections of 94%, 97%, and 98%, respectively, accompanied by large water permeance up to 25 L m^{-2} h^{-1} under low feed pressure of 2 bar, despite the fact that the semi-free spatial swelling of ultrathin GO layer above the substrate pores can deteriorate salt rejection. Our work provides a straightforward physical strategy to adjust the interlayer spacing of the membranes fabricated by two-dimensional nanosheets for achieving desired filtration capacity.

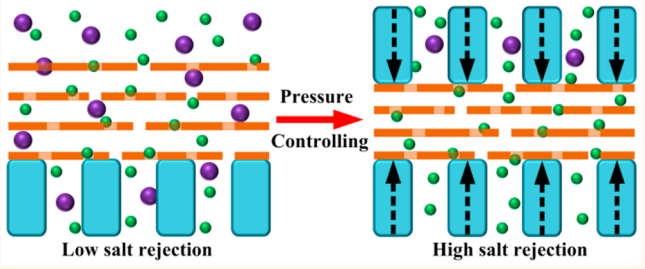

KEYWORDS: *graphene oxide films, interlayer spacing, swelling, membrane separation, desalination, external pressure regulation*

The earth's water is abundant in view of total volume, but the available water is miserably low. Moreover, the maldistribution, the increasing demand, and more contamination of freshwater caused by industrial progress and population growth further aggravate the water scarcity, which could be even worse in the future.[1−4] Water purification, especially desalination to separate salts and other solutes of seawater and brackish water, is of extreme importance for obtaining fresh water. Membrane separation is an energy-efficient and environment-friendly technology for water treatment.[3,4] Various materials, particularly polymers, have been exploited to prepare robust desalination membranes.[4−7] However, the design and preparation of the membranes with high rejection and permeance are still the main developing directions.

Graphene and its derivatives show great potential for fabrication of high-performance membranes due to the extremely thin two-dimensional structure and ultrastrong mechanical strength.[8−19] Nanoporous monolayer graphene membranes display strong mechanical strength, large flux, and high rejection.[20−25] Unfortunately, the complex procedures of pore controlling and high-quality graphene fabrication make these membranes difficult to be scaled up for practical application. The highly processable graphene oxide (GO) membranes derived from GO stacking have outstanding efficiency for removing high-valence ions and small dyes, owing to the sharp size-exclusion from interlayer spacing,[26−30] whereas these membranes exhibit moderate rejection for the main solutes of brackish water and seawater,[26−29] such as sodium, potassium, calcium, magnesium salts, because of the GO swelling. The interlayer spacing will increase to 1.2−1.4 nm with the hydration of GO nanosheets, as investigated by using X-ray diffraction (XRD) characterization.[31−37] Mi *et al.* observed the interlayer spacing even as large as 6.0−7.0 nm, though the technique was based on quartz crystal microbalance and ellipsometry.[38] In order to immobilize the interlayer spacing, some functional molecules have been introduced for cross-linking GO membranes.[39] The intrinsic geometry of the molecules between GO nanosheets makes this method difficult

Received: June 3, 2018
Accepted: September 5, 2018
Published: September 5, 2018

DOI: 10.1021/acsnano.8b04187
ACS Nano 2018, 12, 9309–9317

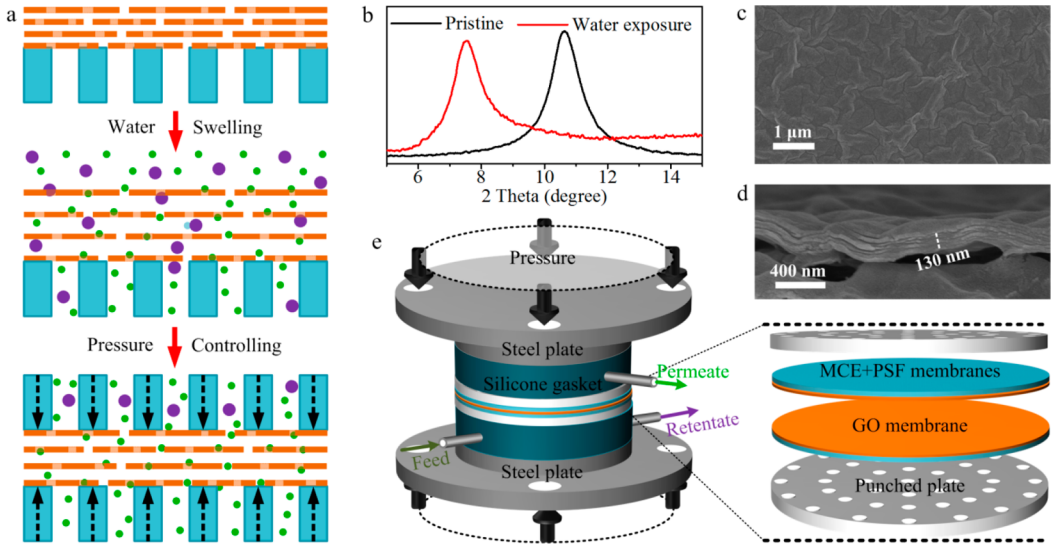

Figure 1. EPR concept for controlling GO interlayer spacing. (a) Schematic of desalination by swelled and compressed GO membranes. GO nanosheets, substrates, water molecules, salts, and external pressure are represented by brown broad lines, cyan rectangles, green dots, purple dots, and black dotted arrows, respectively. (b) XRD patterns of the pristine GO membrane and the GO membrane after wetting in NaCl solution. (c,d) SEM images of top and cross-sectional views of the GO membrane prepared with GO loading, 400 μg. (e) EPR permeation cell for desalination evaluation. MCE and PSF are mixed cellulose ester and polysulfone, respectively.

to obtain small enough interlayer channels for desalination. Reduction of GO by thermal treatment or reagents can tune the interlayer spacing,[40,41] but there is a risk of obtaining an impermeable membrane.[42] Cation-controlling can efficiently enhance the sieving effect of GO membranes for those cations with larger hydrated diameters.[43] Some of the other strategies based on chemistry have also been proposed for better separation performance.[30,44−47]

Beside the chemical strategies, physical pressure methods have been demonstrated with good feasibility to control the interlayer spacing as well. Talyzin *et al.* found that the pressure applied by diamond anvil cell induced the first expansion and then constriction of GO lattice in water, with a maximum of 30%.[48] This phenomenon was also observed when other solvents were applied.[49,50] The negative compressibility was attributed to the insertion of water into interlayer spacing under pressure. On the contrary, some studies reported that the increased feed pressure enhanced slat rejection of GO membranes in the reduced transport channels.[30,51] These divergent results may be caused by the different processes for pressure. Recently, the GO laminates were encapsulated by epoxy at different humidity conditions to adjust the interlayer spacing.[52] The obtained aligned membranes displayed high salt rejection, yet the architecture with vertically aligned GO nanosheets reduced the utilization of GO and the feasibility of scale-up production. Until now, controlling of interlayer spacing of GO membranes is still a great challenge.

Here, we report a concept of external pressure regulation (EPR) to control GO interlayer spacing. Unlike isotropic materials with omnidirectional swelling, the anisotropic GO membranes with two-dimensional configuration almost only swell in the vertical direction. Thus, the swelling can be effectively restrained by externally unidirectional reverse force (Figure 1a). Based on this concept, an EPR system with GO membranes is designed for water desalination by adjusting the high-resolution external pressure. As the result of physical fixation of GO nanosheets, the EPR system can be operated with cross-flow filtration. The rejections of the compressed GO membranes increase from below 20% to 94% (KCl), 97% (NaCl), and 98% ($CaCl_2$), while water permeance maintains as high as 25 L m^{-2} h^{-1} bar^{-1}.

RESULTS AND DISCUSSION

Ultrathin GO membranes supported by mixed cellulose ester substrates with pore size of 220 nm were fabricated by vacuum filtration.[53] XRD results revealed that the pristine GO membrane dried at atmosphere with humidity of 33% possessed an interlayer spacing of 0.83 nm (Figure 1b). After wetting in NaCl solution, the interlayer spacing swelled to 1.17 nm. These two values were consistent with the observations in previous study.[43] Scanning electron microscopy (SEM) images indicated that all membranes with GO loadings of 100 (10 mL, 10 μg mL^{-1}), 400 (10 mL, 40 μg mL^{-1}), and 800 (10 mL, 80 μg mL^{-1}) μg were continuous and had thicknesses of approximately 33, 130, and 250 nm, respectively (Figure 1c,d, and Figures S1 and S2). For verifying the EPR concept, two face-to-face GO membranes were pressed by two punched steel plates (Figure 1e and Figure S3). Two polysulfone ultrafiltration membranes with nonwoven fabric substrates and four mixed cellulose ester microfiltration membranes were equally placed between the GO membranes and the punched steel plates to homogenize the imposed pressure (Figure S4). The external pressure was controlled by adjusting the screw length and monitored by a wheel-type pressure weighing sensor. Two elastic silicone rings were applied as feed and permeate chambers as well as to maintain the external pressure. To avoid the peel-off of GO layers from substrates, the separation property of GO membranes was tested by dead-end filtration or static diffusion in most previous studies.[26−29,40−47,52,54,55] In this study, because GO layers were compacted by the EPR system, the desalination performance was evaluated by using cross-flow filtration that was typically employed for practical application.

The GO membrane with GO loading of 400 μg exhibited ordinary rejection <20% for all KCl, NaCl, and $CaCl_2$ (Figure S5). As expected from the Donnan exclusion theory, the

DOI: 10.1021/acsnano.8b04187
ACS Nano 2018, 12, 9309−9317

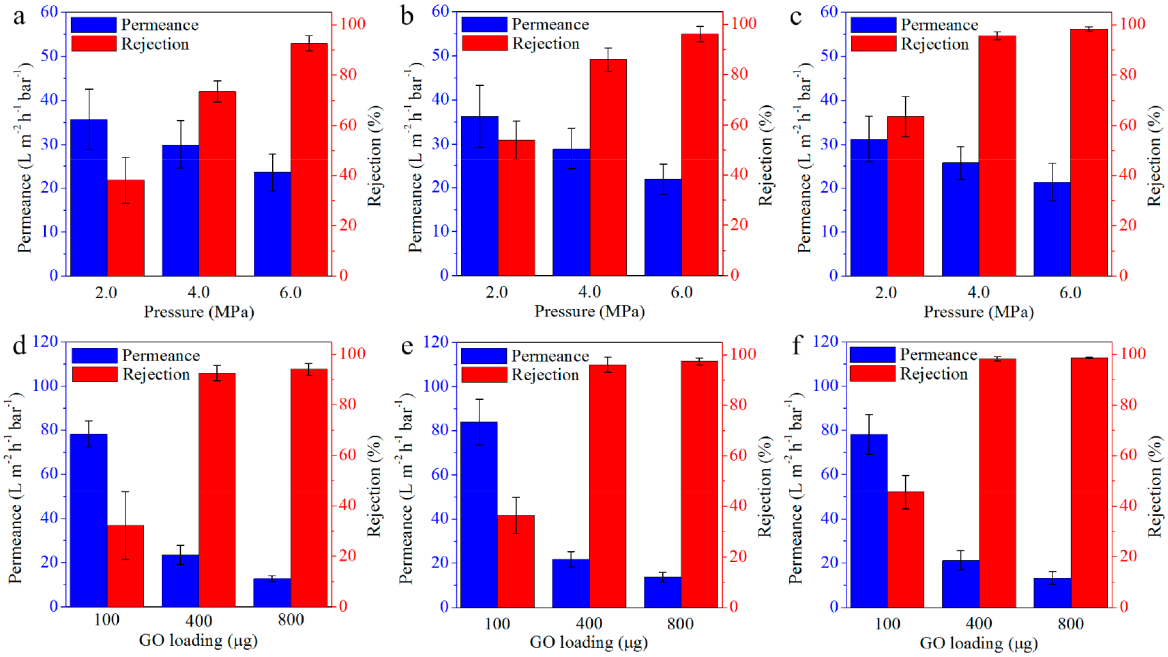

Figure 2. Desalination performance of GO membranes in EPR system. (a–c) Water permeance and KCl, NaCl and $CaCl_2$ rejections of the GO membrane under different external pressures. The 130 nm membrane with GO loading of 400 μg was prepared with a volume of 10 mL and concentration of 40 μg mL^{-1}. (d–f) Water permeance and KCl, NaCl, and $CaCl_2$ rejections of the GO membranes with various loadings and thickness (33, 130, and 250 nm). The applied external pressure was 6.0 MPa.

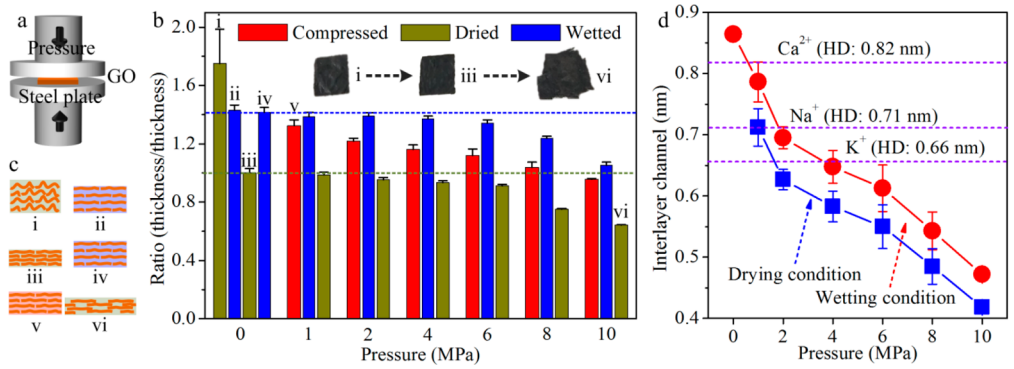

Figure 3. Swelling property of GO membranes under external pressure. (a) Schematic of swelling measurement under external pressure. (b) The normalization thickness of GO flake under compressing, wetting, and drying states. The values were calculated with thickness benchmark of (iii) the redried GO flake. (c) Structural representation of (i) as-synthesized, (ii) wetted, (iii) redried, (iv) rewetted, (v) compressed, and (vi) high-pressure compressed GO flakes. (d) The interlayer channels of the GO flake under various external pressures. The values of the red line were based on the thickness of (iv) the rewetted GO flake, the wetted interlayer spacing, and 0.34 nm thickness of GO. The values of the blue line were based on the thickness of (iii) the redried GO flake, the dried interlayer spacing, and GO thickness.

rejection for different salts had an increasing order as $CaCl_2$, KCl, and NaCl. Figure 2 and Tables S1 and S2 present the water permeance and salt rejections of the GO membranes with various loadings under different external pressures. With the increase of external pressure, the permeance decreased, while rejection increased. This phenomenon was also observed in previous studies; the high feed pressure was applied to enhance the compaction of selective layers for improving the rejection of GO and polymeric membranes.[30,51,56] The result was in line with the shrunken interlayer spacing under pressure. When the external pressure of 6.0 MPa was applied, the salt rejections reached as high as 92.7% (KCl), 96.1% (NaCl), and 98.3% ($CaCl_2$), which increased as the diameter hydrated. These rejections were much higher than those of the GO membranes reported in previous studies.[26,29,30,44] Definitely, the cross-flow filtration used in this study may contribute to obtain the high rejections more or less due to the ameliorated concentration polarization. The increasing rate of rejection for different salts as external pressure was varied. The rejection of larger salt was ameliorated faster than smaller one. These results demonstrated the main rejection mechanism changed from Donnan exclusion based on the negatively charged property of GO membranes to ion sieving, owing to the compressed interlayer spacing. The membranes with NaCl rejection over 95% showed high water permeance of 10–25 L m^{-2} h^{-1} bar^{-1}, which was greater than that of the polymeric membranes with similar salt rejection.[57] We investigated the performance of substrates at external pressure of 6.0 MPa. The low NaCl rejection (<5%) verified that the improved performance should be attributed to the reduced interlayer spacing of GO membranes. As shown in Figure S6, both water and salt permeation rates decreased as pressure increased, but a

DOI: 10.1021/acsnano.8b04187
ACS Nano 2018, 12, 9309–9317

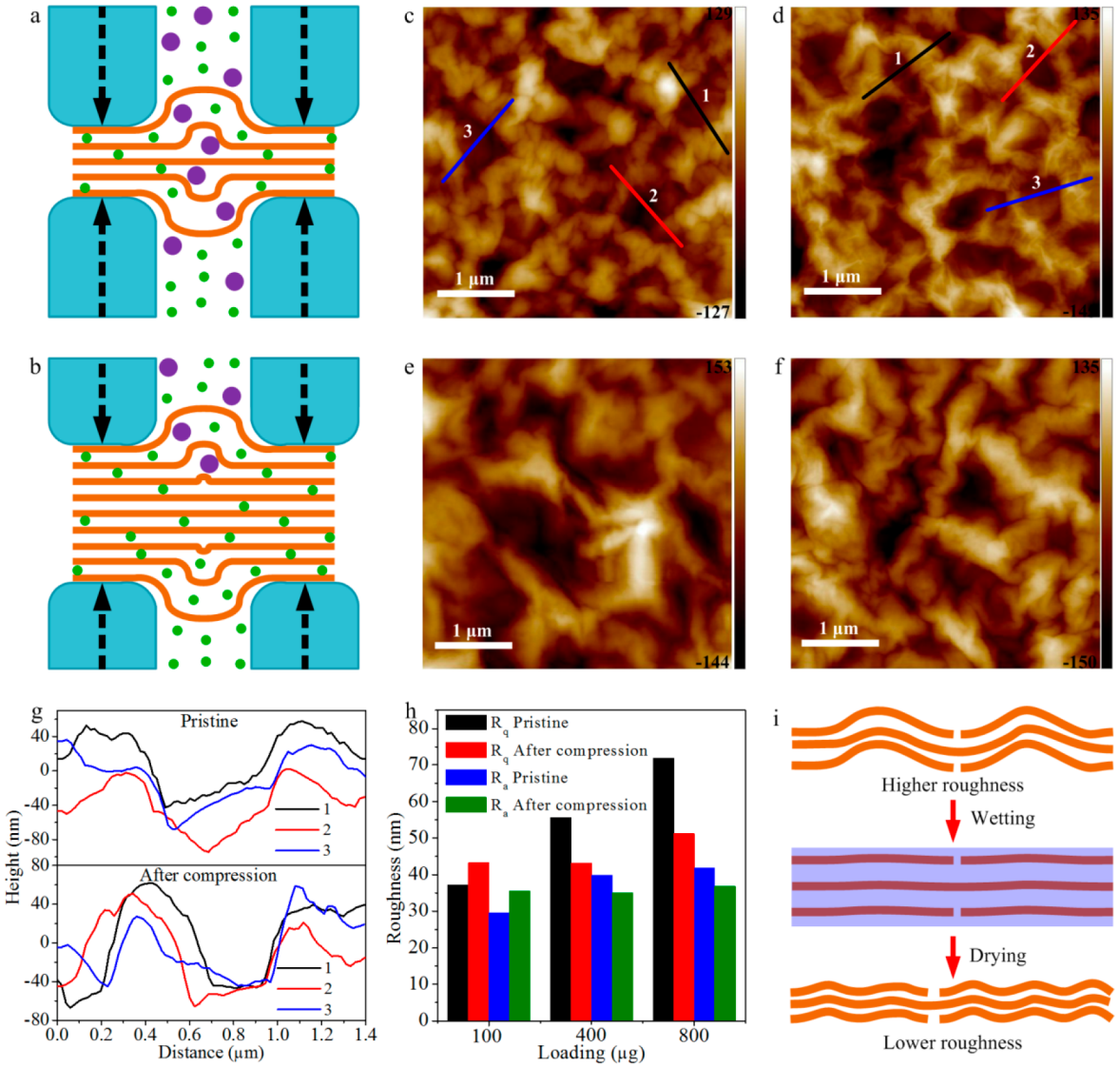

Figure 4. Separation mechanism in EPR system. (a,b) Schematic diagrams of desalination by thin and thick GO membranes. The semi-free GO swelling at substrate pores resulted in inferior rejection. (c–f) AFM images of (c,e) the pristine GO membranes and (d,f) the GO membranes after ERP desalination. The membranes were prepared with GO loadings of (c,d) 100 and (e,f) 400 μg. (g) Height distributions of the GO membranes shown in (c) and (d). (h) R_q and R_a roughness of the GO membranes with loadings of 100, 400, and 800 μg. These values were calculated with 16 μm^2 area. (i) Schematic diagram for the smaller roughness of GO membranes after ERP desalination.

relatively faster decline in salt permeation rates resulted in improvement of water/salt selectivity. The water/KCl, water/NaCl, and water/$CaCl_2$ selectivities increased from 1.2, 1.3, and 1.1 to 15.8, 41.9, and 69.3, respectively. Besides external pressure, membrane thickness also impacted the desalination performance significantly (Figure 2d–f). The rejections and selectivities of the GO membrane with loading of 100 μg were inferior, despite the larger water permeance and permeation rate. This result was attributed to the semi-free swelling of the ultrathin GO membranes, as shown below. Nevertheless, the GO membrane with loading of 800 μg at external pressure of 6.0 MPa showed impressive KCl, NaCl, and $CaCl_2$ rejections of 94.2%, 97.5%, and 98.7%, respectively, with high corresponding water/salt selectivities of 19.4 (KCl), 48.6 (NaCl), and 81.9 ($CaCl_2$). The outstanding desalination performance of GO membranes under external pressure confirmed the availability of EPR concept.

GO swelling property in salt solution was measured under external pressure (Figure 3a,b). The GO flake with thickness of around 200 μm was synthesized by water evaporation.[58] We had tried to fabricate the GO flake with large thickness by vacuum filtration. But it was difficult to obtain the GO flake with thickness of several hundreds of micrometers, because the water permeance decreased dramatically as the thickness increased. The GO flake was first wetted and dried (i) to (iii) between two steel plates. The comparatively smaller interlayer spacing of 0.79 nm calculated from XRD pattern (iii) was resulted from the less interlayer water molecules after vacuum drying at 50 °C (Figure S7). The first wetting (i) to (ii) reduced the thickness dramatically (Figure 3b). This was explained by the fact that the space-free drying process of flake fabrication prompted the formation of some corrugations, which caused the increased apparent thickness (Figure 3c). After rewetting (iii) to (iv), the thickness increased by 41.6%. The dried GO flake had slightly larger experimental thickness

DOI: 10.1021/acsnano.8b04187
ACS Nano 2018, 12, 9309–9317

than the theoretical one due to the small corrugations, meanwhile the wetted flake exhibited similar experimental and theoretical thicknesses due to the relaxing arrangement of GO nanosheets, thus the experimental swelling was smaller than the theoretical one of 47.3% based on the interlayer spacing of wetted and dried GO (Figure S8). By compression, GO swelling could be restrained substantially. The 6.0 MPa external pressure controlled the swelling at 12.0%. After removing the external pressure of 1.0 to 6.0 MPa, the thickness could approximately return to the original value, demonstrating that the GO flake remained an intact structure. It should be noted that the overhigh pressure could cause the permanent thickness reduction of GO flake (vi, shown in Figure 3b,c). The similar XRD patterns of the dried (iii) and redried (vi) samples verified that there was hardly any change in crystalline structure after compression (Figure S7). With the GO nanosheet thickness at 0.34 nm, the GO interlayer channels under drying and wetting conditions were 0.45 and 0.83 nm, respectively. Based on the thickness and interlayer spacing of the dried GO flake (iii), the interlayer channels of GO flake at compressing, wetting,and drying states were calculated (Figure S9). The results showed that the interlayer channel under compression with pressure of 2.0 MPa was smaller than all hydrated diameters of K^+ (0.66 nm), Na^+ (0.71 nm), and Ca^{2+} (0.82 nm) cations.[59] As mentioned above, the corrugations of dried GO flake resulted in obtaining the smaller calculated interlayer channels than actual ones. When calculations were standardized by the thickness and interlayer spacing of the wetted GO flake (iv), the interlayer channel with pressure of 6.0 MPa was narrower than all cations. Since the measuring contact pressure compressed the thickness of wetted GO flake more or less, the actual interlayer channel was smaller than the measured one from XRD, thereby bringing out the slightly bigger calculated interlayer channels than the actual ones under compression. It could be confirmed that the real interlayer channels of the compressed GO were between the two calculated ones (Figure 3d). Because of the permanent thickness reduction, the interlayer channels for the high-pressure compressed GO flakes were underestimated. It should be noted, in hydration of GO, the first water layer for increasing the interlayer spacing to about 0.7−0.8 nm was very stable and difficult to remove, due to the strong hydrogen-bond interaction.[28,38,60] However, the second layer or bilayer waters had good mobility.[28,60−62] This was the reason why all compressed GO flakes had interlayer spacing larger than 0.8 nm, even for the high-pressure compressed ones with much underestimated values. At external pressure of 6.0 MPa, the interlayer spacing decreased to about 0.95 nm, which was close to that of a GO membrane with bilayer waters.

We further investigated the separation mechanism of GO membranes in EPR system. After compression, the indentations from the punching holes on mixed cellulose ester and polysulfone membranes were formed and weakened as closing to GO layer (Figure S4). The flat surface without indentation and the shrinkage of substrates that loaded the GO layers revealed the uniform distribution of pressure on membranes (Figure S10). After drying and tearing off, two GO membranes exhibited chiral photographs (Figure S11a,b). The exposed substrate surface that contacted with GO layer had some residual GO nanosheets (Figure S11d,g). These phenomena proved that two GO layers contacted with each other tightly and uniformly. As the above results of desalination, GO loading influenced the filtration performance drastically. The membrane with a loading of 100 μg displayed a low NaCl rejection of 36.4% under 6.0 MPa pressure. This was interpreted by the semi-free swelling of GO nanosheets at the regions of the submicrometer-sized pores of substrates (Figure 4a). The vacuum filtration for GO deposition provided the superfluous width for curve formation (Figure S2). The pore imprints shown in SEM images and the low-lying regions with a height of about 80 nm presented in atomic force microscopy (AFM) images verified the semi-free swelling basin structures (Figure 4c,d,g, and Figures S2 and S12). It was noteworthy that the basin morphologies became clearer and sharper after desalination in the EPR system (Figure S13). For the membranes with large loadings, although the bottom sides may have basin structures, the top surface displayed the typical wrinkle morphologies due to the GO superposition (Figure 4b,e,f, and Figures S2, S12, and S14), thereby leading to the better rejection. The semi-free swelling was also the reason for the low rejection of the thick membranes that had smaller calculated interlayer channels than cation hydrated diameters, such as, at pressure of 4.0 MPa, the interlayer channel was below 0.65 nm, but the membrane with GO loading of 400 μg exhibited moderate NaCl rejection of 85.9%. Certainly, the wrinkles may also cut down the salt rejection to some extent. Compared with the pristine membranes, the compressed GO membranes with high loadings possessed a smaller roughness (Figure 4h). For example, the root-mean-square roughness (R_q) and arithmetic average roughness (R_a) of the GO membrane with GO loading of 800 μg decreased from 71.8 and 41.8 nm to 51.2 and 36.8 nm, respectively, calculated by 4.0 μm foursquare. AFM images with low magnification showed a similar phenomenon (Figure S15). This was the result when the micrometer-sized wrinkles were compressed to submirometer-sized ones (Figure 4i), verifying the pressure was uniformly applied to whole membranes with high resolution. It is worth mentioning that the AFM characterized the spatial structure of the dried GO membranes after rather than under compression. Because the swelling increased the membrane thickness, the applied external pressure should have a much greater impact on the construction and interlayer spacing of the wetted membranes.

For GO membranes, all inter-edge spaces, inner pores and interlayer channels provided the transport way for molecular diffusion.[26,60−62] The inter-edge spaces and inner pores, which were perpendicular to GO nanosheets, influenced the molecular diffusion greatly.[60] The interlayer channels were much longer and offered selectivity. Because of the thickness of hundreds of nanometers and the constant sizes of perpendicular channels under vertical pressure, the change of interlayer channels under external pressure was considered as the dominant factor for the improved performance. As demonstrated by previous experiments, the rejection increased with feed pressure increase as the compressed interlayer channels.[30,51] But for reported computer simulations, the divergent results were reported. One theory was that the increased pressure reduced the protection of ions from solvation shell, and the dominated interaction between ions and GO walls enhanced the rejections.[63] Another theory deemed that the large pressure overcame the energetic penalty of hydration of ions and peeled off the water molecules from the hydration shell, thereby resulting in poorer salt rejection under higher pressure.[64,65] The different finds from experiments and simulations may be the results of the different executing conditions. For experiments, the feed pressure not only pushed

DOI: 10.1021/acsnano.8b04187
ACS Nano 2018, 12, 9309−9317

water molecules through the membranes but also compressed the interlayer spacing. However, for simulations, the interlayer spacing was set as a certain value for different pressures. Herein, the feed pressure of 2.0 bar for driving the molecules through GO membranes was small and constant. The external pressure, which only compressed GO membranes, was much larger. That was to say, the interlayer spacing could be well compressed by external pressure, yet the low feed pressure could not overcome the energy barrier of the hydration shell. Thus, EPR strategy improved the rejection efficiently. Moreover, smaller interlayer spacing enhanced the free energy barrier for entering or exiting of ions in GO membranes, thereby leading the rejection improvement further.[63] The interlayer spacing showed great effect on water permeance likewise.[62,65−67] The permeance decreased greatly as the interlayer channels narrowed. The interlayer spacing was usually identified by the number of water layers of monolayer, bilayer, and trilayer, as investigated in simulations.[60,62,67] When the interlayer spacing decreased to about 0.7 nm with monolayer water, the water was almost virtually stationary even under external pressure, due to the dominant hydrogen-bond interaction from oxygen-containing groups.[28,36,67] Herein, the interlayer spacing at 6.0 MPa was about 0.95 nm, which was equivalent to that of GO membranes with bilayer waters. Therefore, the membranes displayed good permeance.

Besides the external pressure, semi-free spatial swelling and membrane thickness affect the separation performance of GO membranes as well. The superfluous GO geometric dimensions at the regions of substrate pores led to the curve formation and then prompted the semi-free spatial swelling, consequently causing the poor size-exclusion effect and high permeance. Fortunately, the larger thickness reduced the semi-free spatial swelling of the GO nanosheets that kept relatively away from the substrates and enhanced the rejection, despite the increase of mass transfer resistance of membranes. Because the thickness was smaller than the height of low-lying regions that prompted the semi-free swelling, the GO membrane with thickness of 33 nm exhibited poor rejection even at a high pressure of 6.0 MPa. On the contrary, when the membranes had enough thickness, the semi-free swelling was restrained, and the rejection and permeance increased and decreased with external pressure, such as, at external pressure of 6.0 MPa, the membrane with a thickness of 130 nm showed impressive performance with high KCl (92.7%), NaCl (96.1%), and $CaCl_2$ (98.3%) rejections and water permeance of about 22 L m^{-2} h^{-1} bar^{-1}.

CONCLUSIONS

We have proposed an EPR concept to precisely adjust the interlayer spacing of GO membranes. Because the swelling mainly occurs in a vertical direction due to the anisotropic features of stacked GO films, the interlayer spacing below 1.0 nm can be controlled by reverse force. As the result of physical fixation of GO nanosheets, the EPR system can be operated under cross-flow filtration. By controlling the external pressure, the GO membranes with high salt rejections and large water permeance can be achieved. Based on our findings, the semi-free spatial swelling of thin GO membranes on porous substrates reduces the desalination performance. Theoretically, by using smoother membranes with smaller pores and other fabrication methods without suction force to suppress the semi-free swelling regions, the thinner GO membranes can be employed to obtain higher rejection and permeance. Moreover, besides controlling GO swelling in water for desalination, the strategy described herein may also regulate the transport channels of other two-dimensional materials in both liquid and gas environments for various applications.

EXPERIMENTAL DETAILS

Preparation of GO Membranes. Graphite oxide was prepared by using the typical modified Hummer's method. The prepared graphite oxide (40 mg) was added in water (40 mL) to obtain the GO suspension with concentration of 1.0 mg mL^{-1} by ultrasonic treatment for 2 h. To remove possibly unexfoliated graphite oxide, the obtained GO suspension was treated by centrifugation with 4000 rpm, despite almost no precipitate. The homogeneous GO suspension was diluted to 10, 40, and 80 μg mL^{-1} by deionized water. Mixed cellulose ester microfiltration membrane with pore size of 220 nm was employed as the substrate to support the GO layer. The diluted GO suspension (10 mL) was applied to fabricate the GO membrane by typical vacuum filtration.

Desalination by EPR System. Two face-to-face contacted GO membranes were compressed by punched steel plates. Two polysulfone ultrafiltration membranes with molecular cut off of 10 kDa and four mixed cellulose ester microfiltration membranes were used as a gasket to homogenize the imposed pressure and provide the water passageway. The external pressure was imposed by adjusting the screw length. A wheel-type pressure weighing sensor was employed to monitor the external pressure. Two elastic silicone rings with thickness, inner diameter, and outer diameter of 1.0, 1.5, and 4.0 cm, respectively, were applied as feed and permeate chambers as well as to maintain the pressure. The desalination performance was evaluated by cross-flow filtration with a retentate flow of 40 L h^{-1}. Salt solution with concentration of 0.5 g L^{-1} was pumped into a feed chamber for permeation under a pressure of 2 bar. The permeate liquid was collected, and the retentate liquid flowed back into feed tank. To avoid the peel-off of the GO layer from the substrate, the separation performance of the GO membrane without external pressure was measured by dead-end filtration with effective area. To reduce the effect of concentration polarization, the feed solution was stirred constantly. A conductivity meter was employed to measure salt concentration. Water permeance (L m^{-2} h^{-1} bar^{-1}) was calculated through dividing the permeate volume by the corresponding permeation area, permeation time, and feed pressure. Rejection was calculated by salt concentrations in the feed solution and the permeate solution. Water/salt selectivity was calculated *via* dividing the molar ratio (water to salt) of the permeate solution by the molar ratio (water to salt) of the retentate solution. Measurement was repeated three times each, for three samples and averaged at least.

GO Swelling Property under External Pressure. XRD is a good technique to investigate the interlayer spacing of GO membranes. However, it is very difficult to characterize the GO membrane by XRD under external pressure. Therefore, we employed the typical method to study the swelling properties by measuring the thickness of GO membranes under external pressure. The GO flake was tailored to a foursquare shape with side length of 2 mm and placed between two flat steel discs. The thickness of the flakes was measured by using a contact thickness gauge with contact pressure of 200−300 Pa and accuracy of 1.0 μm. The GO flake was first wetted and dried under contact pressure of 200−300 Pa in vacuum at 50 °C for 12 h. Since the water evaporation led to the increased apparent thickness originating from the formation of some corrugations, the first wetting reduced the thickness of GO flake. The compressing property was investigated by measuring the thickness of GO flakes under external pressure. All drying/redrying processes were performed by thermal treatment at 50 °C in vacuum for 12 h. During all wetting, drying, rewetting, and redrying processes, the slight contact pressure of 200−300 Pa was applied, which reduced the formation of corrugations. The swelling ratio was based on the thickness of the first redried flake. Measurements were repeated three times each, for three samples and averaged at least.

DOI: 10.1021/acsnano.8b04187
ACS Nano 2018, 12, 9309−9317

Characterizations. The morphology of the prepared membranes was observed by using a scanning electron microscope (Ultra-55, Zeiss Co.) with accelerating voltage of 5 kV. The crystalline structure of the samples was investigated by using a X-ray diffractometer (D2 Phaser, Bruker Co.) at 30 kV and 10 mA. For characterization of GO flakes, the dry sample was fabricated by first wetting the obtained flake for 1 h at room temperature and then drying for 12 h at 50 °C. For XRD measurement of the wetted GO flake, the dried sample was further wetted for another 1 h. Surface morphology of the prepared membranes was characterized by using an atomic force microscope (Bioscope Catalyst Nanoscope-V, Bruker, USA). Arithmetic average roughness (R_a) and root-mean-square roughness (R_q) were calculated by using the NanoScope Analysis software.

ASSOCIATED CONTENT

Supporting Information

The Supporting Information is available free of charge on the ACS Publications website at DOI: 10.1021/acsnano.8b04187.

Characterizations (SEM, XRD, and AFM) of GO membranes, estimation of interlayer spacing, and discussion of desalination performance (PDF)

AUTHOR INFORMATION

Corresponding Author

*E-mail: gandeylin@126.com.

ORCID

Wanbin Li: 0000-0003-2460-168X

Author Contributions

W.L. conceived the research idea and formulated the project. W.L., W.W., and Z. L. performed experiments, including fabrication and characterization of GO membranes, design of permeation system, and collection and analysis of permeation data. W.L. wrote the paper.

Notes

The authors declare no competing financial interest.

ACKNOWLEDGMENTS

This work was financially supported by the National Natural Science Foundation of China (grant no. 51708252), the Fundamental Research Funds for the Central Universities (grant no. 21617322), and Jinan University (grant no. 88016674).

REFERENCES

(1) Shannon, M. A.; Bohn, P. W.; Elimelech, M.; Georgiadis, J. G.; Mariñas, B. J.; Mayes, A. M. Science and Technology for Water Purification in the Coming Decades. *Nature* **2008**, *452*, 301−310.

(2) Bolisetty, S.; Mezzenga, R. Amyloid-Carbon Hybrid Membranes for Universal Water Purification. *Nat. Nanotechnol.* **2016**, *11*, 365−371.

(3) Werber, J. R.; Osuji, C. O.; Elimelech, M. Materials for Next-Generation Desalination and Water Purification Membranes. *Nat. Rev. Mater.* **2016**, *1*, 16018.

(4) Chen, W.; Chen, S.; Liang, T.; Zhang, Q.; Fan, Z.; Yin, H.; Huang, K. W.; Zhang, X.; Lai, Z.; Sheng, P. High-Flux Water Desalination with Interfacial Salt Sieving Effect in Nanoporous Carbon Composite Membranes. *Nat. Nanotechnol.* **2018**, *13*, 345−350.

(5) Koros, W. J.; Zhang, C. Materials for Next-Generation Molecularly Selective Synthetic Membranes. *Nat. Mater.* **2017**, *16*, 289−297.

(6) Park, H. B.; Freeman, B. D.; Zhang, Z. B.; Sankir, M.; McGrath, J. E. Highly Chlorine-Tolerant Polymers for Desalination. *Angew. Chem., Int. Ed.* **2008**, *47*, 6019−6024.

(7) Cho, K. L.; Hill, A. J.; Caruso, F.; Kentish, S. E. Chlorine Resistant Glutaraldehyde Crosslinked Polyelectrolyte Multilayer Membranes for Desalination. *Adv. Mater.* **2015**, *27*, 2791−2796.

(8) Liu, G.; Jin, W.; Xu, N. Graphene-Based Membranes. *Chem. Soc. Rev.* **2015**, *44*, 5016−5030.

(9) Sun, P.; Wang, K.; Zhu, H. Recent Developments in Graphene-Based Membranes: Structure, Mass-Transport Mechanism and Potential Applications. *Adv. Mater.* **2016**, *28*, 2287−2310.

(10) Koenig, S. P.; Wang, L.; Pellegrino, J.; Bunch, J. S. Selective Molecular Sieving Through Porous Graphene. *Nat. Nanotechnol.* **2012**, *7*, 728−732.

(11) Kim, H. W.; Yoon, H. W.; Yoon, S. M.; Yoo, B. M.; Ahn, B. K.; Cho, Y. H.; Shin, H. J.; Yang, H.; Paik, U.; Kwon, S.; Choi, J. Y.; Park, H. B. Selective Gas Transport Through Few-Layered Graphene and Graphene Oxide Membranes. *Science* **2013**, *342*, 91−95.

(12) Li, H.; Song, Z.; Zhang, X.; Huang, Y.; Li, S.; Mao, Y.; Ploehn, H. J.; Bao, Y.; Yu, M. Ultrathin, Molecular-Sieving Graphene Oxide Membranes for Selective Hydrogen Separation. *Science* **2013**, *342*, 95−98.

(13) Sun, P.; Zhu, M.; Wang, K.; Zhong, M.; Wei, J.; Wu, D.; Xu, Z.; Zhu, H. Selective Ion Penetration of Graphene Oxide Membranes. *ACS Nano* **2013**, *7*, 428−437.

(14) Huang, K.; Liu, G.; Lou, Y.; Dong, Z.; Shen, J.; Jin, W. A Graphene Oxide Membrane with Highly Selective Molecular Separation of Aqueous Organic Solution. *Angew. Chem., Int. Ed.* **2014**, *53*, 6929−6932.

(15) Sun, P.; Zheng, F.; Zhu, M.; Song, Z.; Wang, K.; Zhong, M.; Wu, D.; Little, R. B.; Xu, Z.; Zhu, H. Selective Trans-Membrane Transport of Alkali and Alkaline Earth Cations Through Graphene Oxide Membranes Based on Cation-π Interactions. *ACS Nano* **2014**, *8*, 850−859.

(16) Lozada-Hidalgo, M.; Hu, S.; Marshall, O.; Mishchenko, A.; Grigorenko, A. N.; Dryfe, R. A. W.; Radha, B.; Grigorieva, I. V.; Geim, A. K. Sieving Hydrogen Isotopes Through Two-Dimensional Crystals. *Science* **2016**, *351*, 68−70.

(17) Wang, L.; Drahushuk, L. W.; Cantley, L.; Koenig, S. P.; Liu, X.; Pellegrino, J.; Strano, M. S.; Bunch, J. S. Molecular Valves for Controlling Gas Phase Transport Made from Discrete Ångström-Sized Pores in Graphene. *Nat. Nanotechnol.* **2015**, *10*, 785−790.

(18) Shen, J.; Liu, G.; Huang, K.; Chu, Z.; Jin, W.; Xu, N. Subnanometer Two-Dimensional Graphene Oxide Channels for Ultrafast Gas Sieving. *ACS Nano* **2016**, *10* (3), 3398−3409.

(19) Zhou, F.; Tien, H. N.; Xu, W. L.; Chen, J. T.; Liu, Q.; Hicks, E.; Fathizadeh, M.; Li, S.; Yu, M. Ultrathin Graphene Oxide-Based Hollow Fiber Membranes with Brush-Like CO_2-Philic Agent for Highly Efficient CO_2 Capture. *Nat. Commun.* **2017**, *8*, 2107.

(20) Surwade, S. P.; Smirnov, S. N.; Vlassiouk, I. V.; Unocic, R. R.; Veith, G. M.; Dai, S.; Mahurin, S. M. Water Desalination Using Nanoporous Single-Layer Graphene. *Nat. Nanotechnol.* **2015**, *10*, 459−464.

(21) O'Hern, S. C.; Jang, D.; Bose, S.; Idrobo, J. C.; Song, Y.; Laoui, T.; Kong, J.; Karnik, R. Nanofiltration Across Defect-Sealed Nanoporous Monolayer Graphene. *Nano Lett.* **2015**, *15*, 3254−3260.

(22) Wang, L.; Williams, C. M.; Boutilier, M. S. H.; Kidambi, P. R.; Karnik, R. Single-Layer Graphene Membranes Withstand Ultrahigh Applied Pressure. *Nano Lett.* **2017**, *17*, 3081−3088.

(23) Jang, D.; Idrobo, J. C.; Laoui, T.; Karnik, R. Water and Solute Transport Governed by Tunable Pore Size Distributions in Nanoporous Graphene Membranes. *ACS Nano* **2017**, *11*, 10042−10052.

(24) Wei, G.; Quan, X.; Chen, S.; Yu, H. Superpermeable Atomic-Thin Graphene Membranes with High Selectivity. *ACS Nano* **2017**, *11*, 1920−1926.

(25) Kidambi, P. R.; Jang, D.; Idrobo, J. C.; Boutilier, M. S. H.; Wang, L.; Kong, J.; Karnik, R. Nanoporous Atomically Thin Graphene Membranes for Desalting and Dialysis Applications. *Adv. Mater.* **2017**, *29*, 1700277.

(26) Han, Y.; Xu, Z.; Gao, C. Ultrathin Graphene Nanofiltration Membrane for Water Purification. *Adv. Funct. Mater.* **2013**, *23*, 3693−3700.

(27) Huang, H.; Song, Z.; Wei, N.; Shi, L.; Mao, Y.; Ying, Y.; Sun, L.; Xu, Z.; Peng, X. Ultrafast Viscous Water Flow Through Nanostrand-Channelled Graphene Oxide Membranes. *Nat. Commun.* **2013**, *4*, 2979.
(28) Joshi, R. K.; Carbone, P.; Wang, F. C.; Kravets, V. G.; Su, Y.; Grigorieva, I. V.; Wu, H. A.; Geim, A. K.; Nair, R. R. Precise and Ultrafast Molecular Sieving Through Graphene Oxide Membranes. *Science* **2014**, *343*, 752−754.
(29) Akbari, A.; Sheath, P.; Martin, S. T.; Shinde, D. B.; Shaibani, M.; Banerjee, P. C.; Tkacz, R.; Bhattacharyya, D.; Majumder, M. Large-Area Graphene-Based Nanofiltration Membranes by Shear Alignment of Discotic Nematic Liquid Crystals of Graphene Oxide. *Nat. Commun.* **2016**, *7*, 10891.
(30) Morelos-Gomez, A.; Cruz-Silva, R.; Muramatsu, H.; Ortiz-Medina, J.; Araki, T.; Fukuyo, T.; Tejima, S.; Takeuchi, K.; Hayashi, T.; Terrones, M.; Endo, M. Effective NaCl and Dye Rejection of Hybrid Graphene Oxide/Graphene Layered Membranes. *Nat. Nanotechnol.* **2017**, *12*, 1083−1088.
(31) Rezania, B.; Severin, N.; Talyzin, A. V.; Rabe, J. P. Hydration of Bilayered Graphene Oxide. *Nano Lett.* **2014**, *14*, 3993−3998.
(32) Talyzin, A. V.; Hausmaninger, T.; You, S.; Szabó, T. The Structure of Graphene Oxide Membranes in Liquid Water, Ethanol and Water-Ethanol Mixtures. *Nanoscale* **2014**, *6*, 272−281.
(33) Talyzin, A. V.; Luzan, S. M.; Szabó, T.; Chernyshev, D.; Dmitriev, V. Temperature Dependent Structural Breathing of Hydrated Graphite Oxide in H_2O. *Carbon* **2011**, *49*, 1894−1899.
(34) You, S.; Yu, J.; Sundqvist, B.; Belyaeva, L. A.; Avramenko, N. V.; Korobov, M. V.; Talyzin, A. V. Selective Intercalation of Graphite Oxide by Methanol in Water/Methanol Mixtures. *J. Phys. Chem. C* **2013**, *117*, 1963−1968.
(35) You, S.; Sundqvist, B.; Talyzin, A. V. Enormous Lattice Expansion of Hummers Graphite Oxide in Alcohols at Low Temperatures. *ACS Nano* **2013**, *7*, 1395−1399.
(36) Lerf, A.; Buchsteiner, A.; Pieper, J.; Schöttl, S.; Dekany, I.; Szabo, T.; Boehm, H. P. Hydration Behavior and Dynamics of Water Molecules in Graphite Oxide. *J. Phys. Chem. Solids* **2006**, *67*, 1106−1110.
(37) Lian, B.; De Luca, S.; You, Y.; Alwarappan, S.; Yoshimura, M.; Sahajwalla, V.; Smith, S. C.; Leslie, G.; Joshi, R. K. Extraordinary Water Adsorption Characteristics of Graphene Oxide. *Chem. Sci.* **2018**, *9*, 5106−5111.
(38) Zheng, S.; Tu, Q.; Urban, J. J.; Li, S.; Mi, B. Swelling of Graphene Oxide Membranes in Aqueous Solution: Characterization of Interlayer Spacing and Insight into Water Transport Mechanisms. *ACS Nano* **2017**, *11*, 6440−6450.
(39) Hung, W. S.; Tsou, C. H.; De Guzman, M.; An, Q. F.; Liu, Y. L.; Zhang, Y. M.; Hu, C. C.; Lee, K. R.; Lai, J. Y. Cross-Linking with Diamine Monomers to Prepare Composite Graphene Oxide-Framework Membranes with Varying d-Spacing. *Chem. Mater.* **2014**, *26*, 2983−2990.
(40) Huang, L.; Li, Y.; Zhou, Q.; Yuan, W.; Shi, G. Graphene Oxide Membranes with Tunable Semipermeability in Organic Solvents. *Adv. Mater.* **2015**, *27*, 3797−3802.
(41) Liu, H.; Wang, H.; Zhang, X. Facile Fabrication of Freestanding Ultrathin Reduced Graphene Oxide Membranes for Water Purification. *Adv. Mater.* **2015**, *27*, 249−254.
(42) Nair, R. R.; Wu, H. A.; Jayaram, P. N.; Grigorieva, I. V.; Geim, A. K. Unimpeded Permeation of Water Through Helium-Leak-Tight Graphene-Based Membranes. *Science* **2012**, *335*, 442−444.
(43) Chen, L.; Shi, G.; Shen, J.; Peng, B.; Zhang, B.; Wang, Y.; Bian, F.; Wang, J.; Li, D.; Qian, Z.; Xu, G.; Liu, G.; Zeng, J.; Zhang, L.; Yang, Y.; Zhou, G.; Wu, M.; Jin, W.; Li, J.; Fang, H. Ion Sieving in Graphene Oxide Membranes *via* Cationic Control of Interlayer Spacing. *Nature* **2017**, *550*, 380−383.
(44) Xu, W. L.; Fang, C.; Zhou, F.; Song, Z.; Liu, Q.; Qiao, R.; Yu, M. Self-assembly: A Facile Way of Forming Ultrathin, High-Performance Graphene Oxide Membranes for Water Purification. *Nano Lett.* **2017**, *17*, 2928−2933.
(45) Cheng, C.; Jiang, G.; Garvey, C. J.; Wang, Y.; Simon, G. P.; Liu, J. Z.; Li, D. Ion Transport in Complex Layered Graphene-Based Membranes with Tuneable Interlayer Spacing. *Sci. Adv.* **2016**, *2*, e1501272.
(46) Liu, J.; Wang, N.; Yu, L. J.; Karton, A.; Li, W.; Zhang, W.; Guo, F.; Hou, L.; Cheng, Q.; Jiang, L.; Weitz, D. A.; Zhao, Y. Bioinspired Graphene Membrane with Temperature Tunable Channels for Water Gating and Molecular Separation. *Nat. Commun.* **2017**, *8*, 2011.
(47) Qi, B.; He, X.; Zeng, G.; Pan, Y.; Li, G.; Liu, G.; Zhang, Y.; Chen, W.; Sun, Y. Strict Molecular Sieving Over Electrodeposited 2D-Interspacing-Narrowed Graphene Oxide Membranes. *Nat. Commun.* **2017**, *8*, 825.
(48) Talyzin, A. V.; Solozhenko, V. L.; Kurakevych, O. O.; Szabó, T.; Dékány, I.; Kurnosov, A.; Dmitriev, V. Colossal Pressure-Induced Lattice Expansion of Graphite Oxide in the Presence of Water. *Angew. Chem., Int. Ed.* **2008**, *47*, 8268−8271.
(49) Talyzin, A. V.; Sundqvist, B.; Szabó, T.; Dékány, I.; Dmitriev, V. Pressure-Induced Insertion of Liquid Alcohols into Graphite Oxide Structure. *J. Am. Chem. Soc.* **2009**, *131*, 18445−18449.
(50) Talyzin, A. V.; Luzan, S. M. Pressure-Induced Insertion of Liquid Acetone into the Graphite Oxide Structure. *J. Phys. Chem. C* **2010**, *114*, 7004−7006.
(51) Wei, Y.; Zhang, Y.; Gao, X.; Yuan, Y.; Su, B.; Gao, C. Declining Flux and Narrowing Nanochannels under Wrinkles of Compacted Graphene Oxide Nanofiltration Membranes. *Carbon* **2016**, *108*, 568−575.
(52) Abraham, J.; Vasu, K. S.; Williams, C. D.; Gopinadhan, K.; Su, Y.; Cherian, C. T.; Dix, J.; Prestat, E.; Haigh, S. J.; Grigorieva, I. V.; Carbone, P.; Geim, A. K.; Nair, R. R. Tuneable Sieving of Ions Using Graphene Oxide Membranes. *Nat. Nanotechnol.* **2017**, *12*, 546−550.
(53) Dikin, D. A.; Stankovich, S.; Zimney, E. J.; Piner, R. D.; Dommett, G. H. B.; Evmenenko, G.; Nguyen, S. T.; Ruoff, R. S. Preparation and Characterization of Graphene Oxide Paper. *Nature* **2007**, *448*, 457−460.
(54) Huang, L.; Chen, J.; Gao, T.; Zhang, M.; Li, Y.; Dai, L.; Qu, L.; Shi, G. Reduced Graphene Oxide Membranes for Ultrafast Organic Solvent Nanofiltration. *Adv. Mater.* **2016**, *28*, 8669−8674.
(55) Yang, Q.; Su, Y.; Chi, C.; Cherian, C. T.; Huang, K.; Kravets, V. G.; Wang, F. C.; Zhang, J. C.; Pratt, A.; Grigorenko, A. N.; Guinea, F.; Geim, A. K.; Nair, R. R. Ultrathin Graphene-Based Membrane with Precise Molecular Sieving and Ultrafast Solvent Permeation. *Nat. Mater.* **2017**, *16*, 1198−1202.
(56) Pendergast, M. T. M.; Nygaard, J. M.; Ghosh, A. K.; Hoek, E. M. V. Using Nanocomposite Materials Technology to Understand and Control Reverse Osmosis Membrane Compaction. *Desalination* **2010**, *261*, 255−263.
(57) Shi, B.; Marchetti, P.; Peshev, D.; Zhang, S.; Livingston, A. G. Will Ultra-High Permeance Membranes Lead to Ultra-Efficient Processes? Challenges for Molecular Separations in Liquid Systems. *J. Membr. Sci.* **2017**, *525*, 35−47.
(58) Chen, C.; Yang, Q. H.; Yang, Y.; Lv, W.; Wen, Y.; Hou, P. X.; Wang, M.; Cheng, H. M. Self-Assembled Free-Standing Graphite Oxide Membrane. *Adv. Mater.* **2009**, *21*, 3007−3011.
(59) Nightingale, E. R., Jr. Phenomenological Theory of Ion Solvation, Effective Radii of Hydrated Ions. *J. Phys. Chem.* **1959**, *63*, 1381−1387.
(60) Wei, N.; Peng, X.; Xu, Z. Understanding Water Permeation in Graphene Oxide Membranes. *ACS Appl. Mater. Interfaces* **2014**, *6*, 5877−5883.
(61) Jiao, S.; Xu, Z. Non-Continuum Intercalated Water Diffusion Explains Fast Permeation through Graphene Oxide Membranes. *ACS Nano* **2017**, *11*, 11152−11161.
(62) Willcox, J. A. L.; Kim, H. J. Molecular Dynamics Study of Water Flow across Multiple Layers of Pristine, Oxidized, and Mixed Regions of Graphene Oxide. *ACS Nano* **2017**, *11*, 2187−2193.
(63) Sun, P.; Ma, R.; Deng, H.; Song, Z.; Zhen, Z.; Wang, K.; Sasaki, T.; Xu, Z.; Zhu, H. Intrinsic High Water/Ion Selectivity of Graphene Oxide Lamellar Membranes in Concentration Gradient-Driven Diffusion. *Chem. Sci.* **2016**, *7*, 6988−6994.

DOI: 10.1021/acsnano.8b04187
ACS Nano 2018, 12, 9309−9317

(64) Chen, B.; Jiang, H.; Liu, X.; Hu, X. Molecular Insight into Water Desalination across Multilayer Graphene Oxide Membranes. *ACS Appl. Mater. Interfaces* **2017**, *9*, 22826−22836.
(65) Dai, H.; Xu, Z.; Yang, X. Water Permeation and Ion Rejection in Layer-by-Layer Stacked Graphene Oxide Nanochannels: A Molecular Dynamics Simulation. *J. Phys. Chem. C* **2016**, *120*, 22585−22596.
(66) Chen, B.; Jiang, H.; Liu, X.; Hu, X. Observation and Analysis of Water Transport through Graphene Oxide Interlamination. *J. Phys. Chem. C* **2017**, *121*, 1321−1328.
(67) Willcox, J. A. L.; Kim, H. J. Molecular Dynamics Study of Water Flow Across Multiple Layers of Pristine, Oxidized, and Mixed Regions of Graphene Oxide: Effect of Graphene Oxide Layer-to-Layer Distance. *J. Phys. Chem. C* **2017**, *121*, 23659−23668.

DOI: 10.1021/acsnano.8b04187
ACS Nano 2018, 12, 9309−9317